Theoretical Chemistry Accounts (2020) 139:155
https://doi.org/10.1007/s00214-020-02670-4

REGULAR ARTICLE

Theoretical analysis of the influence of C–H···O bonds on the NMR constants of uracil in DMSO

Rodrigo Gester[1] · Ramiro S. Galeano Carrano[2] · Patricio F. Provasi[3] · Carlos Bistafa[4] · Sylvio Canuto[4]

Received: 3 April 2020 / Accepted: 29 August 2020 / Published online: 9 September 2020

Abstract
We combined different models of solvation and density functional theory calculations to study the magnetic properties of uracil in the liquid dimethyl sulfoxide environment. Special attention was paid to the effect of weak hydrogen bonds formation. In uracil, C=O groups act as hydrogen acceptors while N–H is hydrogen donor. The influence in the intramolecular coupling involving the acceptor and donor sites in uracil is perceptible. The ^1J(C,O) and ^1J(N,H) coupling constants decrease by ca. 1.5 Hz and 2.3 Hz, respectively. This behavior depends on the nature of the hydrogen-bonding interaction and cannot be neglected. The best agreement between theory and experiment for the magnetic shielding was obtained using long-range or dispersion corrected exchange-correlation functional such as LC-BLYP, B97D, and ωB97XD. In the particular case of uracil, we concluded that the most important contribution to the calculated magnetic shielding for C–H···O interactions comes from electrostatic contributions.

Keywords Magnetic shielding · Spin–spin coupling · QM/MM methods · Solvent effects · Hydrogen bonds · DFT methods · Dispersion correction · Long-range interactions

1 Introduction

A hydrogen bond is normally defined as an X–H···Y interaction, where X and Y might be some electronegative elements such as N, O, or F [1]. These conventional structures have importance in many biological processes, stabilizing, for instance, the DNA double helix pattern, determining the three-dimensional structure of folded proteins and enzymes, besides being responsible for the unique characteristic of water.

✉ Rodrigo Gester
gester@unifesspa.edu.br

Sylvio Canuto
canuto@if.usp.br

[1] Faculdade de Física, Universidade Federal do Sul e Sudeste do Pará, Marabá, PA 68507-590, Brazil

[2] Facultad de Ciencias Exactas, Químicas y Naturales, Universidad Nacional de Misiones, Posadas, Argentina

[3] Department of Physics, IMIT, CONICET, Northeastern University, AV. Libertad 5500, W 3404 AAS Corrientes, Argentina

[4] Instituto de Física, Universidade de São Paulo, Rua do Matão 1371, São Paulo, SP 05588-090, Brazil

A conventional X–H···Y bond is experimentally characterized by an increase in the X–H bond and a lowering of the frequency of its vibrational stretching modes. However, Trudeau and co-workers [2] established a new baseline for such intermolecular interactions presenting the possibility of the formation of unconventional bonds between solute and solvent molecules. Such structures show C–H···Y (Y = π, N, O, F) conformation, and in contrast to the common hydrogen bonds, they are remarkable by a lowering in the C–H bond and an enlargement in its corresponding stretching frequencies.

The discovery of these new interactions has a direct impact on organic chemistry, where methyl groups are abundant. For these reasons, many efforts were made in an attempt to understand the nature of such interactions. In this sense, significant contributions were made by Hobza [3–7] and Scheiner [8–11], who have studied the origins of the so-called improper C–H blue shift, as well as the role of the unconventional hydrogen bonds in structural chemistry [12, 13].

Despite the advances in the field, for a long time, the existence of unconventional C–H···O bonds were seen as a challenge for Nuclear Magnetic Resonance (NMR), which is one of the most popular techniques for structural

characterization used in organic chemistry. From the ^{1}H, ^{13}C, and ^{15}N NMR parameters, it is possible to obtain useful information about the molecular structure. However, these elements are not very sensitive to the environment when compared to ^{17}O [14], which would be a logical alternative as a structural probe. However, in opposition to the convenience of being a common element in organic compounds, oxygen has particularities that prevent its use in NMR, and the characterization of unconventional C–H···O bonds. Perhaps the major one is the low natural abundance (0.037%) of ^{17}O, the only one with nonzero nuclear spin. Nevertheless, modern instrumentation combined with a smart choice of experimental setup (solvent, pulse reception time, temperature, and concentration) could provide spectra with good resolution for a variety of organic compounds [15].

Once the experimental barriers were overcome, the next step would be to learn how to model such interactions. As most experiments are made in solution, molecular modeling techniques that account for the solute–solvent interactions gain special importance. Interesting results have been obtained combining clusters models to continuum solvent approaches [16, 17]. However, the use of clusters does not include the statistical description necessary for characterizing a liquid system. Another important aspect in NMR is the electronic solute polarization due to solvent. As it was previously discussed, the solute polarization changes the coordination number of solvent molecules around the solute [18–21]. These changes in the chemical environment have influence on NMR spectra, so the inclusion of the solute-polarization effects is necessary, especially in the case of electronegative compounds as nitrogen and oxygen atoms, since they are susceptible to hydrogen bonds.

From the point of view of quantum chemistry, density functional theory (DFT) [22, 23] has been frequently employed due to its satisfactory cost performance. However, a systematic account of dispersion forces, lacking in the most conventional exchange-correlation functionals, remains a challenge. Since dispersive interactions may significantly contribute to several molecular properties, efforts have been made to address these limitations, giving rise to new exchange-correlation functionals [24–26]. Improved functionals have been used to study vibrational frequencies [27–30], ionization [31] and binding energies [32–34]. Although these recent advances allowed treating the weak C–H···Y structures, the effects of weak interactions on specific molecular properties such as the NMR constants remain unclear.

Within these context, uracil is an interesting example because of its biological importance [35–37]. This nucleobase pairs with adenine in ribonucleic acid, and its derivatives are often used as pharmacological agents [37]. In water solvent, uracil makes a strong O–H_{water} ···O_U bond. Experimental works report, in aqueous environment, shielding constants of 55.5 ppm and − 13.5 ppm, respectively, for O1 and O2 (labels are shown in Fig. 1 [38]. Now, in dimethyl sulfoxyde (DMSO), the oxygen atoms of uracil interact with the solvent by a weak and unconventional C–H_{DMSO} ···O_U hydrogen bond, which changes significantly the ^{17}O shielding constants to 35.0 ppm and − 46.5 ppm [39], in comparison with the in-water results. This clearly indicates that the nature of the hydrogen bond interaction has strong influence on the ^{17}O magnetic constants. This demands theoretical attention and is the subject of the present investigation.

In this work, we study the NMR constants of uracil in DMSO solution. We include the electronic polarization of the solute using an iterative process, successfully used before [18–21]. Next, we analyze the influence of the unconventional C–H···O bonds on uracil NMR constants. DFT functionals were combined with different models of solvation to describe environmental effects. Contrary to possible expectations, our results indicate that dispersion forces are not fundamental in the NMR parameters of unconventional C–H···O bonds in uracil, but the use of long-range corrected DFT functionals provided a better understanding of the experimental results. We have considered not only the chemical shielding parameters but also the spin–spin coupling constants. This includes the important intermolecular couplings involved in the hydrogen bonds. The solvent effects on the spin–spin couplings are found to be mild but to depend on the donor and acceptor character of the solute–solvent hydrogen bond. As we will discuss, the $^{1h}J(H_{DMSO},O_U)$ coupling constant across unconventional HBs are two orders of magnitude smaller than conventional $^{1h}J(H_U,O_{DMSO})$ coupling. Shielding and spin–spin coupling constants related to unconventional and weak C–H···O interactions are mainly affected by electrostatic interaction.

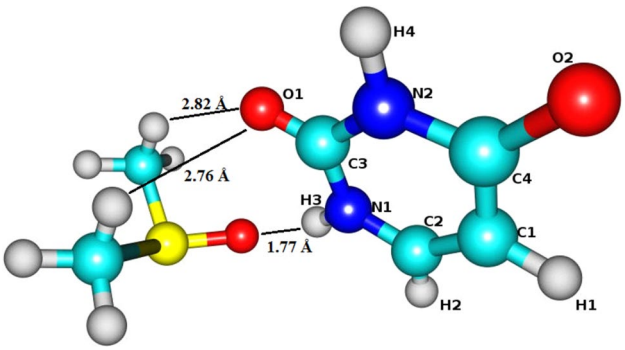

Fig. 1 One of the 100 bonded structures sampled from MC simulations used in the quantum mechanical calculations

2 Computational details

To generate solute–solvent configurations we used Metropolis Monte Carlo simulations. All simulations were performed using the DICE [40] code in the *NpT* ensemble at 1 atm, 398 K and in a cubic box composed by 1 uracil and 500 DMSO molecules. These configurations are sampled for the subsequent quantum mechanics calculations following the sequential quantum mechanics/molecular mechanics methodology (S-QM/MM) [41, 42]. The intermolecular interaction is described by the Lennard–Jones (LJ) plus Coulomb potential. For uracil, we adopted the LJ parameters of the OPLS force field [43]. The charges were obtained after the solute polarization [18–21] calculated using CHELPG fittings [44] of the molecular potential at MP2/aug-cc-pVTZ level of theory. For DMSO, we adopted the all-atom force field proposed by Zhang et al. [45]. The MC simulations were performed in two stages: a thermalization followed by a production stage of 12×10^7 MC steps in thermodynamic equilibrium. More details about the MC simulations can be obtained from our previous works [41, 42]. The iterative scheme to obtain the solute polarization is also described in detail [46]. Uracil and DMSO geometries were both obtained at MP2/aug-cc-pVTZ level of theory.

The NMR calculations use different solvation models. The simple model including only the electrostatic part of the solute–solvent uses the averaged solvent electrostatic configuration (ASEC) [47]. The solvent effects on the calculated nuclear magnetic constants were accounted for by considering both continuum and discrete models of solvent. For the continuum approach, we used the polarizable continuum model (PCM) within the integral equation formalism (IEF-PCM) [48]. Three different models were used as discrete solvent approaches. First, the ASEC model (aforementioned) where the solvent molecules are treated only as simple point charges, and next a micro-hydration shell (HB) including explicitly the water molecules that are involved in hydrogen bonds, as illustrated in Fig. 1. In the third model, explicit hydrogen-bonded DMSO molecules are supplemented by an electrostatic embedding (HB + PC) composed of all the remaining solvent molecules treated as simple point charges. This third model (HB + PC) includes electrostatic bulk effects. While ASEC includes only electrostatic interactions, the HB + PC includes additional contribution such as dispersion interaction of the solute and the nearest solvent molecules. The HB corresponds to all hydrogen-bonded solute–solvent structures sampled from MC simulations. In this case, the results were obtained as averages over 100 snapshots.

To identify the hydrogen bonds, we used both geometrical and energetic criteria [49–51]. The geometrical criterion is obtained from the radial distribution function and the energetic one from the pairwise energy interaction [51]. Hence, we use here $r(X_{solute} \cdots Y_{DMSO}) \leq 4.0$ Å, $E \leq -4.0$ kcal/mol and θ [X–(YH)] $\leq 40.0°$. Using these criteria, only 10% of the MC structures analyzed showed the absence of hydrogen bonds, whereas 42% and 48% of these configurations presented one and two solute–solvent bonds, respectively. O1 participates in 80% of the bonds, while O2 in 58%. Nonconventional hydrogen bonds are more weak interactions. This has direct consequence in the geometric parameters of the hydrogen bond. Figure 1 shows one of these structures sampled from our MC simulations and defines the labels for uracil atoms. Analyzing this liquid structure, it can be noted that the bonds lengths $r(O_{solute} \cdots H_{DMSO})$ ~ 2.8 Å are 60% larger than conventional $r(H_{solute} \cdots O_{DMSO})$ length, confirming that improper hydrogen bonds are weaker interactions.

The quantum mechanical calculations were carried out using the Gaussian 09 [52] and DALTON [53] programs and used different DFT exchange correlations. A very large selection of functional has been adopted. We have used more conventional hybrid models (B3LYP [54, 55], BLYP [54, 55], X3LYP [56], B3PW91 [54, 57], and mPW1PW91 [58]), long-range corrected (CAM-B3LYP [59] and LC-BLYP [60]), pure M06L [61], dispersion-corrected (ωB97XD [24] and B97D [25]) and semi-empirical GGA-type functionals (KT2 [62] and KT3 [63]). The shielding constants were obtained using the Pople 6-311++G(*d,p*) basis set [64–66] within the gauge-independent atomic orbital [67] method. For the spin–spin coupling constants, we used the specially designed aug-pcJ-1 [68] basis set. Finally, the experimental chemical shifts δ were converted to chemical shielding scale by using the Wasylishen and Bryce relation ($\sigma = 287.5$ ppm $- \delta$) [69].

3 Results and discussion

3.1 Solute polarization

The results for the dipole moment after the solute electronic polarization are shown in Table 1 and was obtained at the MP2/aug-cc-pVTZ level of theory. For isolated uracil, we obtained a dipole moment of 4.34 D [19]. This result is in good agreement with the previous theoretical results of 4.39 D [70] but overestimates the experimental prediction of 3.87 D [71].

In DMSO, the iterative procedure converges to a dipole moment of 5.34 D, an increase of 23%. For comparison, Table 1 also shows the result in water using the same procedure. As expected, the dipole moment in water is larger than in DMSO, following the increase in polarity and dielectric

Table 1 The uracil dipole moment (μ/D) in water and DMSO solvents calculated at MP2/aug-cc-pVTZ level of theory:

Isolated molecule		DMSO		Water	
Calculated	Experimental	PCM	Iterative	PCM	Iterative
4.34[a], 4.39 [70]	3.87 [71]	6.02[a]	5.34[a]	6.03 [19]	6.36, 6.45 [19], and 7.01 [70]

PCM means the polarizable continuum model used within the integral equation formalism [48]

[a]This work

Table 2 The ^{17}O magnetic shielding constants (σ/ppm) calculated for uracil in DMSO using the 6-311++G(*d,p*) basis set and different DFT functionals

DFT	O1	O2
B3LYP	23.2 ± 10 (22.1)	− 57.1 ± 1.2 (− 62.8)
X3LYP	23.3 ± 1.0 (22.3)	− 57.1 ± 1.2 (− 62.8)
B3PW91	26.1 ± 1.0 (24.3)	− 54.2 ± 1.2 (− 60.4)
mPW1PW91	27.6 ± 1.0 (27.4)	− 52.0 ± 1.0 (− 59.2)
BLYP	19.4 ± 1.0 (19.3)	− 60.7 ± 1.2 (− 64.8)
ωB97XD	31.8 ± 1.0 (29.8)	− 46.7 ± 1.2 (− 53.5)
B97D	32.9 ± 1.0 (31.8)	− 44.0 ± 1.1 (− 48.4)
CAM-B3LYP	29.0 ± 1.0 (25.8)	− 50.7 ± 1.2 (− 57.3)
LC-BLYP	34.8 ± 1.1 (32.2)	− 45.9 ± 1.3 (− 54.3)
M06L	55.7 ± 0.8 (51.2)	− 13.1 ± 1.0 (− 32.3)
KT2	43.8 ± 0.0 (43.8)	− 29.9 ± 1.1 (− 33.2)
KT3	45.1 ± 0.9 (45.1)	− 28.1 ± 1.1 (− 31.2)
Exp. [39]	35.0	− 46.5

Results obtained using HB + PC model are averaged over 100 configurations. In parentheses, values obtained by using the electrostatic ASEC model

constant. The PCM result shows a larger polarization in DMSO but is unable to distinguish it from the results in water. This pattern was also observed for the case of 5-fluorouracil in acetonitrile [72]. The solute–solvent structures obtained in the iterative procedure were used to calculate the NMR parameters of solvated uracil.

3.2 ^{17}O magnetic shielding

The ^{17}O shielding constants of uracil in DMSO have been reported experimentally by Blicharska and Kupka [39] as 35.0 ppm for O1 and − 46.5 ppm for O2.

Table 2 shows the calculated values for the shielding constants using twelve DFT functionals. For simplicity, we consider only the performances of the HB + PC and ASEC models, and the the role of the exchange and correlation terms of the density functionals could be observed. As both B97D and ωB97XD functionals and the HB + PC model include some dispersion interaction, one may suppose that the good agreement with the experiment must be due to dispersion interactions dominating unconventional C–H···O bonds. The B3LYP functional is probably the most popular exchange-correlation density functional used in quantum chemistry and predicts 23.2 ± 1.0 ppm and − 57.1 ± 1.2 ppm for O1 and O2, respectively, which are the same results obtained with the X3LYP functional. These functionals differ only in the exchange term, which suggests that the electronic correlation should be more relevant for shielding constants. We confirm this statement, by using B3PW91 and mPW1PW91, which differ only by the exchange term. These functionals present the values of 26.1 ± 1.0 and 27.6 ± 1.0 ppm for O1 and − 54.2 ± 1.2 and − 52.0 ± 1.0 ppm for O2. So, the substitution of the exchange term does not affect significantly the shielding constants.

This dependency with respect to the correlation term is better noted comparing the B3PW91 and B3LYP methods. In comparison with the experimental data, it is clear that the B3PW91 correlation functional improves the B3LYP results.

However, a better description is obtained after the inclusion of different forms of long-range corrections. For instance, the Coulomb attenuating method (CAM-B3LYP) improves substantially the B3LYP description predicting 29.0 ± 1.0 ppm and − 50.7 ± 1.2 ppm, respectively, for O1 and O2. And the simple BLYP method only matches the experimental reports after the inclusion of long-range corrections (LC-BLYP), which points out 34.8 ± 1.1 and − 45.9 ± 1.3 ppm for O1 and O2, and shows the importance of long-range corrections for these properties.

The KT2 and KT3 functionals were developed for the study of magnetic properties [62, 63]. Even so, they did not show good performance. The M06L functional produces unsatisfactory results. A possible explanation is that this exchange-correlation approximation was developed especially to deal with transition metals, inorganic, and organometallic materials [61]. The results of Table 2 indicate the importance of long-range and dispersion-corrected models for describing the ^{17}O shielding constants of uracil. The best results are obtained with the LC-BLYP, ωB97XD and B97D models, but the KT2 and KT3 functionals also provide a faithful description of the phenomenon. This idea is better realized in Fig. 2, which plots the relative shielding ($\sigma_{DFT} - \sigma_{exp}$). The smaller bars indicate better theory-experiment accordance.

Now, we analyze the sole contribution of electrostatic interaction. Table 2 also shows, in parentheses, the calculations including the electrostatic ASEC model where no

Table 3 ^{17}O magnetic shielding constants (σ/ppm) calculated for solvated uracil at B97D/6-311++G(*d,p*) level of theory

Atom	Gas	PCM	ASEC	HB	HB + PC (HB + PCM)	Exp. [39] [a]
σ(O1)	15.2	42.7	31.8	19.2 ± 0.8	32.9 ± 1.0 (38.8 ± 0.6)	35.0
$\Delta\sigma$		27.5	16.6	4 ± 0.8	17.7 ± 1.0 (23.6 ± 0.6)	19.8
%		180.9	109.2	26.3	116.4 (155.3)	130.3
σ(O2)	− 81.9	− 31.9	− 48.4	− 60 ± 0.9	− 44 ± 1.1 (− 28.9 ± 0.5)	− 46.5
$\Delta\sigma$		− 50	− 33	− 33.5	− 37.9 ± 1.1 (− 53 ± 0.5)	− 35.4
%		61	40.3	40.9	46.3 (64.7)	43.1

The values of HB, HB + PC and HB + PCM are averages over 100 statistically uncorrelated configurations sampled from the MC simulation

[a]The experimental estimation for $\Delta\sigma$ and % are in relation to the gas-phase values for the ^{17}O shielding constants

[b]PCM means the polarizable continuum model used within the integral equation formalism [48]

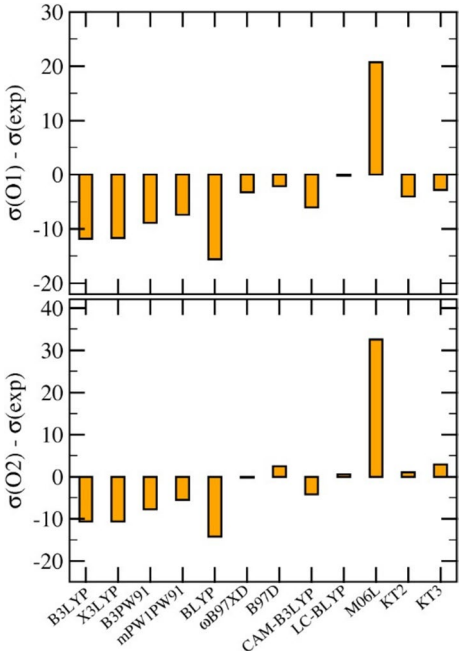

Fig. 2 The relative ($\sigma_{DFT} - \sigma_{exp}$) shielding constant calculated at DFT/6-311++ G(*d,p*) level of theory. The minor barriers indicate better agreement with the experiment

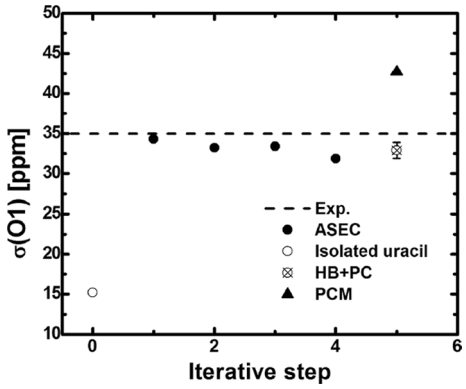

Fig. 3 The ^{17}O shielding constants calculated for different solvation models at B97D/6-311++G(*d,p*) level of theory

solvent molecule is explicitly considered but used as a simple point charge. The dispersion or long-range corrected DFT-based methods show good agreement when applied in the ASEC model. As an example, the calculations with the B97D functional give a magnetic shielding constant of 31.8 ppm for O1 and − 48.4 ppm for O2, a minor decrease compared to the values obtained with the HB + PC model. A similar conclusion is obtained using the LC-BLYP and ωB97XD functionals. However, we noted that the difference between the ASEC and HB + PC models is less pronounced for O1 than for O2. The success of LC-BLYP and CAM-B3LYP using the ASEC model indicates that intermolecular dispersion interaction is small, and the shielding is dominated by the electrostatic interaction. Figure 3 shows the evolution of the shielding constants as a function of the iterative step and stresses the importance of the solute polarization due to solvent. In addition, as we observed before, ASEC and HB + PC present similar results, and both are able to obtain good agreement with the experimental values.

The solvent effect ($\Delta\sigma$) can be obtained taking the difference between the property calculated in solvent and in vacuum conditions. For ^{17}O, such properties are shown in Table 3, and for simplicity, we only discuss the B97D/6-311++G(*d,p*) results.

We could not find experimental reports for the ^{17}O shielding constants of uracil in vacuum. However, our theoretical calculations estimate values of 15.2 ppm and − 81.9 ppm, respectively, for O1 and O2 atomic sites. In DMSO solution, Blicharska and Kupka [39] reported values of 35 ppm and − 46.5 ppm, which indicates a tuning effect of up to 130% for σ(O1) and 43% for σ(O2).

Concerning the solvent models used, the PCM overestimates the experiment and predicts shielding constants of 42.7 ppm on O1, and − 31.9 ppm for O2, respectively. On the other hand, a discussion considering only the

hydrogen-bonded solute–solvent molecules is unsatisfactory. In fact, in contrast to PCM, the HB model underestimated the experiment and predicts unreasonable values, 19.2 ± 0.8 ppm for O1 and − 60 ± 0.9 ppm for O2.

NMR shielding constants are suitably described combining explicit solute–solvent and electrostatic interactions [73]. For instance, Mennucci [16] and Cossi and Crescenzi [17] have improved both, the HB and PCM results embedding some solute–solvent hydrogen-bonded structures in a continuum environment (HB + PCM). By using this model, we obtained the O1 shielding constant as 38.8 ± 0.6 ppm, but a less consistent value of − 28.9 ± 0.5 ppm for O2. Very good results were obtained with the HB + PC model providing the best agreement with the experimental values, 32.9 ± 1.0 ppm and − 44.0 ± 1.1 ppm for O1 and O2, respectively. Good results were also obtained for the ωB97XD functional, which is corrected for dispersion forces, obtaining the values of 31.8 ± 1.0 ppm for O1 and − 46.7 ± 1.2 ppm for O2 (see Table 2).

These findings for uracil illustrate the relevance of ^{17}O NMR for the structural characterization of natural products or biological compounds. For aprotical nitrogen systems such as pyridine and pyrazines, σ(N) suffers a reasonable gas–solvent shift ranging from 10 to 30% [74]. Minor effects (ca. 9%) are reported for protic nitrogen systems [21]. On the other hand, with respect to the vacuum, our HB + PC solvation model indicates a solvent effect of ca. 130% for σ(O). Therefore, ^{17}O NMR parameters may be an excellent probe to measure structural changes in the chemical environment.

3.3 Spin–spin coupling constants

Now, we will consider the indirect spin–spin constants J, and for the atomic labels, refer to Fig. 1. The solvent effects on intramolecular ^1J(N1,H3), ^1J(N2,H4), ^1J(C3,O1), and ^1J(C4,O2) coupling constants are of particular importance because they are directly involved in solute–solvent hydrogen bond interactions. Whereas ^1J(N1,H3) and ^1J(N2,H4) constants describe hydrogen-bond donor sites, ^1J(C3,O1) and ^1J(C4,O2) are related to hydrogen-bond acceptors. Keal and collaborators [75] have studied the ^1J(N,H) and ^1J(C,O) constants and found good results for a variety of molecular systems using the B97-2 and B97-3 functionals. Based on their results, our calculations were carried out at B97D/aug-pcJ-1 level of theory using the HB + PC solvent model. The results are organized in Table 4. The B97D functional can be considered an improvement of the B97-2 and B97-3 methods by partially including dispersion corrections.

In **T**able 4, we note that the effect of the solvents are small, but systematic. For instance, for isolated uracil ^1J(N1,H3) is − 95.1 Hz, whereas the PCM model point out the value of − 97.4 Hz, i.e., a solvent effect of ca. 2.3 Hz. After the inclusion of the explicit solvent molecules by using the HB model, this value becomes − 97.6 Hz. This agreement with PCM indicates that the major contribution for ^1J(N1,H3) comes from the nearest solvent molecules. In fact, this statement becomes clear when we consider the HB + PC model. The inclusion of the remaining molecules through point charges does not affect ^1J(N1,H3), which is estimated as − 97.4 ± 0.1 Hz.

Table 4 Intramolecular spin–spin coupling constants (J/Hz) calculated for solvated uracil at B97D/aug-pcJ-1 level of theory

Coupling	Gas	PCM	ASEC	HB	HB + PC
^1J(N1,H3)	− 95.1	− 97.4	− 97.6	− 97.0 ± 0.1	− 97.4 ± 0.1
^1J(N2,H4)	− 89.8	− 89.4	− 90.1	− 90.5 ± 0.1	− 89.8 ± 0.1
^1J(C3,O1)	25.5	22.8	23.7	24.1 ± 0.1	23.2 ± 0.1
^1J(C6,O2)	26.2	23.3	24.8	25.3 ± 0.1	24.7 ± 0.1

HB and HB + PC are averages over 100 statistically uncorrelated configurations sampled from the MC simulation

[a]PCM means the polarizable continuum model used within the integral equation formalism [48]

The other coupling constant, ^1J(N2,H4), is even less affected by the environment. Under gaseous conditions, this coupling is estimated as − 89.8 Hz. However, our most complete model, HB + PC, shows an imperceptible change, indicating a coupling of − 89.8 ± 0.1 Hz.

These findings lead us to discuss the flexibility of uracil and its impact on nuclear couplings. Contrary to one might expected, uracil is a flexible molecule when compared to other pyrazine rings [76, 77]. However, the current values do not account for environmental effects on the solute structure, but as the solvent shift ΔJ is quite small, it is important to discuss how such effects could impact our results. Recently, Roohi and Nokhostin studied the NMR chemical shielding and spin–spin coupling constants across hydrogen bonds in uracil–α-hydroxy-*N*-nitrosamine complexes [78]. Such results accounted for geometry relaxation effects, and the ^1J(N,H) couplings showed small solvent effects, which also decreases this magnetic constant, corroborating our current results. As the main conclusion, ^1J(N,H) in uracil shows little dependence relative to possible structural changes mediated by the solvent.

Concerning the gaseous-phase conditions, similar results are obtained for the ^1J(C3,O1) coupling constants at the carbonyl active sites. For instance, the HB + PC model presents a value of 23.2 ± 0.1 Hz, which means a solvation effect of ca. − 2.3 ± 0.1 Hz. The ^1J(C4,O2) constant also follows this tendency and decreases ca. − 1.5 ± 0.1 Hz. The PCM and ASEC models give results in close agreement with those obtained using the HB + PC solvent models. In turn, using only the HB to represent the solvent seems also to obtain good results. Although the differences among these three models are less than 1.0 Hz, it indicates that specifically for

^1J(C,O) couplings, electrostatic interactions are the dominant forces.

The same behavior is found for other ^1J(C,O) coupling in carbonyl function. For hydrated tartaric acid, for instance, after considering the solute relaxation in the presence of the solvent, Fideles et al. [79] obtained solvent effects of ca. − 2.5 Hz for ^1J(C,O) coupling when there is the formation of C–O···H bonds. For uracil and accounting for effects of geometry, Roohi and Nokhostin found the same effect for ^1J(C,O) [78].

Our current results even without considering the influence of the solvent on the solute geometry agree with experimental and theoretical evidence and predict the correct trend for the solvent effect either for ^1J(N,H) and ^1J(C,O) couplings. Moreover, these results reinforce that the major contribution for such NMR properties in uracil comes from the solute polarization due to the surrounding.

Figure 4 translates the central idea of the iterative procedure. From gaseous (step 0) to solvent conditions (step 1–5), both ^1J(N2,H4) and ^1J(C3,O1) become more negative. However, a minimal number of MC simulations are necessary to ensure the convergence for such parameters. Although one spends some time performing a series of MC simulations, the desired property is obtained by building an ASEC and performing only one QM calculation, avoiding the computational time ordered by the HB + PC, which includes explicit solvent molecules.

Since NMR parameters are important in bio-molecular characterization and because of the size of such systems, the ASEC model presents a low-demanding computational alternative for calculating the solvent effects. The PCM model is also seen to give a good numerical representation and the correct trend.

Now, we consider the intermolecular couplings across the hydrogen bonds formed between uracil and DMSO. The

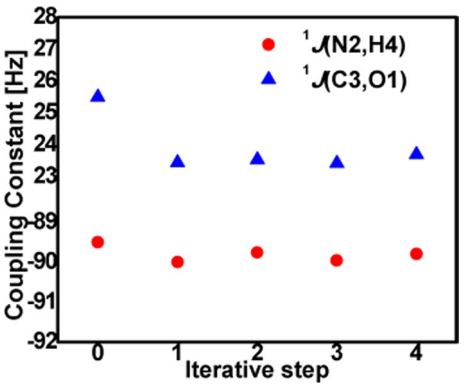

Fig. 4 The intramolecular ^1J(N2,H4) and ^1J(C3,O1) coupling constants of uracil in DMSO calculated at B97D/aug-pcJ-1 level of theory, as a function of the iterative step

Table 5 Intermolecular spin–spin coupling constants (*J*/Hz) calculated for solvated uracil at B97D/aug-pcJ-1 level of theory

Across N–H···O bonds	HB	HB + PC
$^{1h}J(H3_U,O_{DMSO})$	4.9 ± 0.2	5.3 ± 0.2
$^{1h}J(H4_U,O_{DMSO})$	4.2 ± 0.1	4.8 ± 0.1

HB and HB + PC are averages over 100 statistically uncorrelated configurations sampled from the MC simulation

results are shown in Table 5. $^{1h}J(H3_U,O_{DMSO})$ and $^{1h}J(H4_U,O_{DMSO})$ are coupling constants directly related to intermolecular HBs. The calculated values using B97D/aug-pcJ-1 are 4.9 ± 0.2 Hz for $^{1h}J(H3_U,O_{DMSO})$ and 4.2 ± 0.1 Hz for $^{1h}J(H4_U,O_{DMSO})$ using only DMSO molecules that are hydrogen bonded to uracil. Using, in addition, the electrostatic embedding, the HB + PC model, we obtain 5.3 ± 0.2 Hz for $^{1h}J(H3_U,O_{DMSO})$ and 4.8 ± 0.1 Hz for $^{1h}J(H4_U,O_{DMSO})$. This is an increase of only ~ 0.5 Hz between the HB and HB + PC. These values are different from conventional single bond ^1J(O,H) constants. For uracil in water, it has been reported values from − 79 Hz (vapor) to − 89.8 and − 96 Hz (liquid). For pure methanol and ethanol ^1J(O,H) is reported, respectively, as − 83 and − 83.5 Hz [80]. As expected, the solvent effect caused by non-conventional HB in intermolecular couplings is much smaller than the regular HB, but it is perceptible and should not be ignored when accounting spin–spin couplings of molecules even in weak interacting solvents.

4 Conclusions

Various exchange-correlation functionals in density functional theory and different models of solvation have been considered in calculating NMR magnetic shieldings and spin–spin coupling constants for uracil in DMSO. The solute polarization by the solvent changes the uracil dipole moment from 4.34 to 5.34 D and influences the NMR constants. The magnetic shielding exhibits stronger sensitivity concerning the solvent interaction than the spin–spin coupling constants. Oxygen atoms in uracil interact with DMSO by unconventional C–H···O bonds, but even this weak hydrogen bond causes strong solvent shifts (~ 40 ppm) in ^{17}O shielding constants. This feature makes this molecular property useful to study the liquid environment. Furthermore, it is important to account the long-range corrections to describe shielding constants properly in unconventional C–H···O hydrogen bonds. Very good agreement between theory and experiment was obtained using the long-range LC-BLYP, the dispersion-corrected B97D, and ωB97XD functionals considering solvent with explicit DMSO molecules directly

involved in hydrogen bonds supplemented by the electrostatic embedding obtained from the remaining solvent molecules (the HB + PC solvation model). The results of 34.8 ± 1.1 ppm and − 45.9 ± 1.3 ppm for O1 and O2, respectively, obtained with the B96D/6-311++G(*d,p*) model are in very good agreement with the corresponding experimental values of 35.0 ppm and − 46.5 ppm.

The influence of the solvent on the single-bonded spin–spin coupling constants ^1J(N1,H3), ^1J(N2,H4), ^1J(C3,O1), and ^1J(C4,O2) were also considered. It is found that all coupling constants become more negative when a hydrogen bond is formed.

Acknowledgements The authors thank the Brazilian funding agencies CAPES (Coordenação de Aperfeiçoamento de Pessoal de Nível Superior), CNPq (Conselho Nacional de Desenvolvimento Científico e Tecnológico) and FAPESP (Fundação de Apoio à Pesquisa do Estado de São Paulo) This work has also been partially supported by the Institute of Complex Fluids (INCT-FCx). P.F.P. acknowledges financial support from CONICET and UNNE (PI: 17/F207 Res. 966/17 C.S.).

References

1. Arunan E, Desiraju GR, Klein RA, Sadlej J, Scheiner S, Alkorta I, Clary DC, Crabtree RH, Dannenberg JJ, Hobza P, Kjaergaard HG, Legon AC, Mennucci B, Nesbitt DJ (2011) Defining the hydrogen bond: an account (IUPAC technical report). Pure Appl Chem 83(8):1619
2. Trudeau G, Dumas JM, Dupuis P, Guérin M, Sandorfy C (1980) Topics in current chemistry. Springer, Berlin, pp 91–125
3. Hobza P, Havlas Z (2000) Blue-shifting hydrogen bonds. Chem Rev 100(11):4253
4. van der Veken BJ, Herrebout WA, Szostak R, Shchepkin DN, Havlas Z, Hobza P (2001) The nature of improper, blue-shifting hydrogen bonding verified experimentally. J Am Chem Soc 123(49):12290
5. Reimann B, Buchhold K, Vaupel S, Brutschy B, Havlas Z, Špirko V, Hobza P (2001) Improper, blue-shifting hydrogen bond between fluorobenzene and fluoroform†. J Phys Chem A 105(23):5560
6. Hobza P, Havlas Z (2002) Improper, blue-shifting hydrogen bond. Theor Chem Acc Theory Comput Model (Theor Chim Acta) 108(6):325
7. Chocholoušová J, Špirko V, Hobza P (2004) First local minimum of the formic acid dimer exhibits simultaneously red-shifted o-h···o and improper blue-shifted c-h···o hydrogen bonds. Phys Chem Chem Phys 6(1):37
8. Gu Y, Kar T, Scheiner S (1999) Fundamental properties of the CH···o interaction: Is it a true hydrogen bond? J Am Chem Soc 121(40):9411
9. Scheiner S, Grabowski SJ, Kar T (2001) Influence of hybridization and substitution on the properties of the CH···o hydrogen bond. J Phys Chem A 105(46):10607
10. Scheiner S, Kar T, Gu Y (2001) Strength of the $C^{\alpha}H\cdot O$ hydrogen bond of amino acid residues. J Biol Chem 276(13):9832
11. Scheiner S, Kar T (2002) Red- versus blue-shifting hydrogen bonds: Are there fundamental distinctions? J Phys Chem A 106(9):1784
12. Hermansson K (2002) Blue-shifting hydrogen bonds. J Phys Chem A 106(18):4695
13. Pejov L, Hermansson K (2003) On the nature of blueshifting hydrogen bonds: ab initio and density functional studies of several fluoroform complexes. J Chem Phys 119(1):313
14. Boykin DW (1995) In: Structure and chemistry (Part D). Elsevier, pp 549–600
15. Macomber RS (1998) A complete introduction to modern NMR spectroscopy, 1st edn. Wiley, New York
16. Mennucci B (2002) Hydrogen bond versus polar effects: an ab initio analysis on $n-\pi^*$ absorption spectra and n nuclear shieldings of diazines in solution. J Am Chem Soc 124(7):1506
17. Cossi M, Crescenzi O (2004) Solvent effects on ^{17}O nuclear magnetic shielding: N-methylformamide in polar and apolar solutions. Theor Chem Acc 111(2–6):162
18. Gester RM, Georg HC, Fonseca TL, Provasi PF, Canuto S (2012) A simple analysis of the influence of the solvent-induced electronic polarization on the ^{15}N magnetic shielding of pyridine in water. Theor Chem Acc 131(5):117–124
19. Gester RM, Bistafa C, Georg HC, Coutinho K, Canuto S (2013) Theoretically describing the ^{17}O magnetic shielding constant of biomolecular systems: uracil and 5-fluorouracil in water environment. Theor Chem Acc 133(1):1424
20. Manzoni V, Lyra ML, Gester RM, Coutinho K, Canuto S (2010) Study of the optical and magnetic properties of pyrimidine in water combining PCM and QM/MM methodologies. Phys Chem Chem Phys 12(42):14023
21. Gester RM, Georg HC, Canuto S, Caputo MC, Provasi PF (2009) NMR chemical shielding and spin–spin coupling constants of liquid NH3: a systematic investigation using the sequential QM/MM method†. J Phys Chem A 113(52):14936
22. Hohenberg P, Kohn W (1964) Inhomogeneous electron gas. Phys Rev 136(3B):B864
23. Kohn W, Sham LJ (1965) Self-consistent equations including exchange and correlation effects. Phys Rev 140(4A):A1133
24. Chai JD, Head-Gordon M (2008) Long-range corrected hybrid density functionals with damped atom–atom dispersion corrections. Phys Chem Chem Phys 10(44):6615
25. Grimme S (2006) Semiempirical GGA-type density functional constructed with a long-range dispersion correction. J Comput Chem 27(15):1787
26. Zhao Y, Truhlar DG (2007) The m06 suite of density functionals for main group thermochemistry, thermochemical kinetics, noncovalent interactions, excited states, and transition elements: two new functionals and systematic testing of four M06-class functionals and 12 other functionals. Theor Chem Acc 120(1–3):215
27. Takahashi M, Ishikawa Y, Ito H (2012) The dispersion correction and weak-hydrogen-bond network in low-frequency vibration of solid-state salicylic acid. Chem Phys Lett 531:98
28. Babu KR, Vaitheeswaran G (2013) Lattice dynamics and electronic structure of energetic solids LiN3 and NaN3: a first principles study. Chem Phys Lett 586:44
29. Pedone A, Presti D, Menziani MC (2012) On the ability of periodic dispersion-corrected DFT calculations to predict molecular crystal polymorphism in para-diiodobenzene. Chem Phys Lett 541:12
30. Biczysko M, Panek P, Barone V (2009) Toward spectroscopic studies of biologically relevant systems: Vibrational spectrum of adenine as a test case for performances of long-range/dispersion corrected density functionals. Chem Phys Lett 475(1–3):105
31. Rob F, Szalewicz K (2013) Asymptotic dispersion energies from distributed polarizabilities. Chem Phys Lett 572:146
32. Lin H, Zhu SG, Zhang L, Peng XH, Chen PY, Li HZ (2012) Intermolecular interactions, thermodynamic properties, crystal structure, and detonation performance of HMX/NTO cocrystal explosive. Int J Quantum Chem 113(10):1591
33. Liu X, Bereźniak T, Panek JJ, Jezierska-Mazzarello A (2013) Theoretical study of zeatin—a plant hormone and potential drug

for neural diseases—on the basis of DFT, MP2 and target docking. Chem Phys Lett 557:140
34. Pankewitz T, Klopper W (2010) Interaction of the alcohol molecules methanol and ethanol with single-walled carbon nanotubes—a computational study. Chem Phys Lett 498(4–6):345
35. Janke EMB, Weisz K (2013) Low-temperature NMR studies on the geometry of base pairs involving 5-substituted uracil derivatives. J Phys Chem B 117(17):4853
36. Bocchino C, Carabellese A, Caruso T, Sala GD, Ricart S, Spinella A (2014) Preparation of pyrimidin-2-one derivatives via base-mediated decomposition of uracil-analogues fischer carbene complex. J Organomet Chem 749:47
37. Longley DB, Harkin DP, Johnston PG (2003) 5-fluorouracil: mechanisms of action and clinical strategies. Nat Rev Cancer 3(5):330
38. Chandrasekaran S, Wilson WD, Boykin DW (1985) Oxygen-17 NMR studies on 5-substituted uracils. J Org Chem 50(6):829
39. Blicharska B, Kupka T (2002) Theoretical DFT and experimental NMR studies on uracil and 5-fluorouracil. J Mol Struct 613(1–3):153
40. Coutinho K, Canuto S (2003) Dice: A Monte Carlo program for molecular liquid simulation
41. Coutinho K, Canuto S, Zerner MC (2000) A Monte Carlo-quantum mechanics study of the solvatochromic shifts of the lowest transition of benzene. J Chem Phys 112(22):9874
42. Rivelino R, Cabral BC, Coutinho K, Canuto S (2005) Electronic polarization in liquid acetonitrile: a sequential monte carlo/quantum mechanics investigation. Chem Phys Lett 407(1–3):13
43. Pranata J, Wierschke SG, Jorgensen WL (1991) OPLS potential functions for nucleotide bases relative association constants of hydrogen-bonded base. Pairs in chloroform. J Am Chem Soc 113(8):2810
44. Breneman CM, Wiberg KB (1990) Determining atom-centered monopoles from molecular electrostatic potentials. The need for high sampling density in formamide conformational analysis. J Comput Chem 11(3):361
45. Zhang Q, Zhang X, Yu L, Zhao DX (2009) Polarizable force field for water-dimethyl sulfoxide systems: I parameterization and gas phase test. J Mol Liq 145(2):58
46. Georg HC, Coutinho K, Canuto S (2006) Converged electronic polarization of acetone in liquid water and the role in the n-$^{\pi}*$ transition. Chem Phys Lett 429(1–3):119
47. Coutinho K, Georg H, Fonseca T, Ludwig V, Canuto S (2007) An efficient statistically converged average configuration for solvent effects. Chem Phys Lett 437(1–3):148
48. Miertuš S, Scrocco E, Tomasi J (1981) Electrostatic interaction of a solute with a continuum. a direct utilizaion of ab initio molecular potentials for the prevision of solvent effects. Chem Phys 55(1):117
49. Stillinger FH, Rahman A (1972) Molecular dynamics study of temperature effects on water structure and kinetics. J Chem Phys 57(3):1281
50. Mezei M, Beveridge DL (1981) Monte carlo studies of the structure of dilute aqueous sclutions of li^+, na^+, k^+, f^-, and cl^-. J Chem Phys 74(12):6902
51. Canuto S, Coutinho K (2000) From hydrogen bond to bulk: solvation analysis of the $n-\pi^*$ transition of formaldehyde in water. Int J Quantum Chem 77(1):192
52. Frisch MJ, Trucks GW, Schlegel HB, Scuseria GE, Robb MA, Cheeseman JR, Scalmani G, Barone V, Mennucci B, Petersson GA, Nakatsuji H, Caricato M, Li X, Hratchian HP, Izmaylov AF, Bloino J, Zheng G, Sonnenberg JL, Hada M, Ehara M, Toyota K, Fukuda R, Hasegawa J, Ishida M, Nakajima T, Honda Y, Kitao O, Nakai H, Vreven T, Montgomery JA Jr, Peralta JE, Ogliaro F, Bearpark M, Heyd JJ, Brothers E, Kudin KN, Staroverov VN, Kobayashi R, Normand J, Raghavachari K, Rendell A, Burant JC, Iyengar SS, Tomasi J, Cossi M, Rega N, Millam JM, Klene M, Knox JE, Cross JB, Bakken V, Adamo C, Jaramillo J, Gomperts R, Stratmann RE, Yazyev O, Austin AJ, Cammi R, Pomelli C, Ochterski JW, Martin RL, Morokuma K, Zakrzewski VG, Voth GA, Salvador P, Dannenberg JJ, Dapprich S, Daniels AD, Farkas C, Foresman JB, Ortiz JV, Cioslowski J, Fox DJ (2009) Gaussian-09 Revision E.01. Gaussian Inc, Wallingford CT
53. Aidas K, Angeli C, Bak KL, Bakken V, Bast R, Boman L, Christiansen O, Cimiraglia R, Coriani S, Dahle P, Dalskov EK, Ekström U, Enevoldsen T, Eriksen JJ, Ettenhuber P, Fernández B, Ferrighi L, Fliegl H, Frediani L, Hald K, Halkier A, Hättig C, Heiberg H, Helgaker T, Hennum AC, Hettema H, Hjertenaes E, Høst S, Høyvik IM, Iozzi MF, Jansík B, Jensen HJA, Jonsson D, Jørgensen P, Kauczor J, Kirpekar S, Kjaergaard T, Klopper W, Knecht S, Kobayashi R, Koch H, Kongsted J, Krapp A, Kristensen K, Ligabue A, Lutnaes OB, Melo JI, Mikkelsen KV, Myhre RH, Neiss C, Nielsen CB, Norman P, Olsen J, Olsen JMH, Osted A, Packer MJ, Pawlowski F, Pedersen TB, Provasi PF, Reine S, Rinkevicius Z, Ruden TA, Ruud K, Rybkin VV, Sałek P, Samson CCM, de Merás AS, Saue T, Sauer SPA, Schimmelpfennig B, Sneskov K, Steindal AH, Sylvester-Hvid KO, Taylor PR, Teale AM, Tellgren EI, Tew DP, Thorvaldsen AJ, Thøgersen L, Vahtras O, Watson MA, Wilson DJD, Ziolkowski M, Ågren H (2013) The dalton quantum chemistry program system, Wiley interdisciplinary reviews: computational molecular. Science 4(3):269
54. Becke AD (1988) Density-functional exchange-energy approximation with correct asymptotic behavior. Phys Rev A 38(6):3098
55. Lee C, Yang W, Parr RG (1988) Development of the colle-salvetti correlation-energy formula into a functional of the electron density. Phys Rev B 37(2):785
56. Xu X, Goddard WA (2004) From the cover: the x3lyp extended density functional for accurate descriptions of nonbond interactions, spin states, and thermochemical properties. Proc Natl Acad Sci 101(9):2673
57. Becke AD (1993) Density-functional thermochemistry. III. The role of exact exchange. J Chem Phys 98(7):5648
58. Adamo C, Barone V (1998) Exchange functionals with improved long-range behavior and adiabatic connection methods without adjustable parameters: The mPW and mPW1pw models. J Chem Phys 108(2):664
59. Yanai T, Tew DP, Handy NC (2004) A new hybrid exchange-correlation functional using the coulomb-attenuating method (CAM-b3lyp). Chem Phys Lett 393(1–3):51
60. Iikura H, Tsuneda T, Yanai T, Hirao K (2001) A long-range correction scheme for generalized-gradient-approximation exchange functionals. J Chem Phys 115(8):3540
61. Zhao Y, Truhlar DG (2006) A new local density functional for main-group thermochemistry, transition metal bonding, thermochemical kinetics, and noncovalent interactions. J Chem Phys 125(19):194101
62. Keal TW, Tozer DJ (2003) The exchange-correlation potential in Kohn-Sham nuclear magnetic resonance shielding calculations. J Chem Phys 119(6):3015
63. Keal TW, Tozer DJ (2004) A semiempirical generalized gradient approximation exchange-correlation functional. J Chem Phys 121(12):5654
64. Krishnan R, Binkley JS, Seeger R, Pople JA (1980) J Chem Phys 72:650
65. McLean AD, Chandler GS (1980) J Chem Phys 72:5639
66. Blaudeau JP, McGrath MP, Curtiss LA, Radom L (1997) J Chem Phys 107:5016
67. Wolinski K, Hinton JF, Pulay P (1990) Efficient implementation of the gauge-independent atomic orbital method for NMR chemical shift calculations. J Am Chem Soc 112(23):8251

68. Jensen F (2008) Basis set convergence of nuclear magnetic shielding constants calculated by density functional methods. J Chem Theory Comput 4(5):719
69. Wasylishen RE, Bryce DL (2002) A revised experimental absolute magnetic shielding scale for oxygen. J Chem Phys 117(22):10061
70. Ludwig V, Coutinho K, Canuto S (2007) A monte carlo-quantum mechanics study of the lowest $n-\pi^*$ and $\pi-\pi^*$ states of uracil in water. Phys Chem Chem Phys 9(35):4907
71. Brown RD, Godfrey PD, McNaughton D, Pierlot AP (1988) Microwave spectrum of uracil. J Am Chem Soc 110(7):2329
72. Bistafa C, Canuto S (2012) Solvent effects on the two lowest-lying singlet excited states of 5-fluorouracil. Theor Chem Acc 132(1)
73. Buckingham AD, Schaefer T, Schneider WG (1960) Solvent effects in nuclear magnetic resonance spectra. J Chem Phys 32(4):1227
74. Modesto-Costa L, Gester RM, Manzoni V (2017) The role of electrostatic interactions and solvent polarity on the ^{1}5N NMR shielding of azines. Chem Phys Lett 686:189
75. Keal TW, Helgaker T, Sałek P, Tozer DJ (2006) Choice of exchange-correlation functional for computing NMR indirect spin–spin coupling constants. Chem Phys Lett 425(1–3):163
76. Shishkin OV, Gorb L, Leszczynski J (2009) Practical aspects of computational chemistry. Springer, Berlin, pp 399–413
77. Shishkin OV, Gorb L, Luzanov AV, Elstner M, Suhai S, Leszczynski J (2003) Structure and conformational flexibility of uracil: a comprehensive study of performance of the MP2, B3LYP and SCC-DFTB methods. J Mol Struct (Thoechem) 625(1–3):295
78. Roohi H, Nokhostin R (2013) NMR chemical shielding and spin–spin coupling constants across hydrogen bonds in uracil-$^{\alpha}$-hydroxy-n-nitrosamine complexes. Struct Chem 25(2):483
79. Fideles B, Oliveira LB, Colherinhas G (2016) GIAO-DFT isotropic magnetic shielding constants and spin-spin coupling of tartaric acid in water solution. Chem Phys Lett 644:205
80. Gerothanassis IP (2010) Oxygen-17 NMR spectroscopy: basic principles and applications (part II). Prog Nucl Magn Reson Spectrosc 57(1):1